How hazardous are tsunamis triggered by small-scale mass-wasting events on volcanic islands? New insights from Madeira – NE Atlantic

R. Omira [a,b,*], M.A. Baptista [b,c], R. Quartau [d,a], R.S. Ramalho [e,a,f,g], J. Kim [b], I. Ramalho [a,b], A. Rodrigues [d]

[a] *Instituto Dom Luiz (IDL), Faculdade de Ciências, Universidade de Lisboa, Lisbon, Portugal*
[b] *Instituto Português do Mar e da Atmosfera (IPMA), Lisbon, Portugal*
[c] *Instituto Superior de Engenharia de Lisboa, ISEL, Instituto Politécnico, Lisbon, Portugal*
[d] *Instituto Hidrográfico, Lisbon, Portugal*
[e] *School of Earth and Environmental Sciences, Cardiff University, Park Place, Cardiff, CF10 3AT, UK*
[f] *School of Earth Sciences, University of Bristol, Wills Memorial Building, Queen's Road, Bristol BS8 1RJ, UK*
[g] *Lamont-Doherty Earth Observatory, Columbia University, Comer Geochemistry Building, PO Box 1000, Palisades, NY10964-8000, USA*

A B S T R A C T

Mass-wasting events are a key process in the evolution of volcanic ocean islands. They occur at various dimensional scales and present a major source of hazard. When the collapsed material plunges into the sea, destructive tsunamis can be generated. Yet, the hazard potential of collapse-induced tsunamis is still poorly understood with different opinions on what consequences to expect from this type of events, particularly those related to massive volcanic island flank collapses. In this paper, however, we explore the hazard extent of tsunamis triggered by the smaller – but more frequent – coastal cliff-failures, in order to isolate critical factors in the generation, propagation and impact of these tsunamis. To achieve this, we use the prime example of Madeira, a volcanic island in the Atlantic Ocean highly vulnerable to cliff-failure. Particularly, we explore the March 4th, 1930 Cabo Girão event that triggered a deadly tsunami. The coastal impact of the 1930 "Deadly Wave", as the island's inhabitants referred to the generated tsunami, resulted in 19 fatalities. We use historical description, morphological analysis, and numerical modelling to better understand the tsunamigenesis of tall island cliffs failing into the sea. Interestingly, we find that a relatively small-scale mass-wasting event ($\sim$0.003 km^3 volume) was the cause of the reported tsunami that inundated the nearest coasts. Our numerical results, fairly agreeing with the available collapse and subsequent tsunami descriptions, suggest that the tsunami impact was mainly localized on the southern coast of Madeira Island. Furthermore, our study allows proposing a novel morphology-based conceptional model for the tsunamigenesis and hazard extent induced by mass-wasting events on oceanic volcanic islands.

© 2021 Elsevier B.V. All rights reserved.

1. Introduction

Volcanic ocean islands are very prominent and dynamic structures involving continuous stages of construction and destruction (e.g., McGuire, 1996; Ramalho et al., 2013). Throughout their lifecycles, mass-wasting events often interrupt the growth of the islands by removing significant parts of their edifices (e.g., Carracedo, 1996; Moore et al., 1994). These episodes present a major source of hazard in volcanic islands as they can involve large volumes of material and generate fast running debris avalanches (Siebert, 1992). If the failure material plunges into the sea, it can generate destructive tsunami that can potentially affect communities and infrastructure along low-lying coasts (e.g., McGuire, 2006).

Evidence of possibly catastrophic mass-wasting events in volcanic islands has been revealed in numerous studies (Moore et al., 1994; Carracedo, 1999; Day et al., 1999; Quartau et al., 2018a). Some research works linked the collapses to the generation of tsunamis (McGuire, 2006; Paris et al., 2011; Watt et al., 2012; Omira et al., 2016a). Exceptionally, McMurtry et al. (2004), Pérez-Torrado et al. (2006), Paris et al. (2017), and Ramalho et al. (2015a) described deposits that attest to the impact of megatsunamis following catastrophic collapses of Mauna Loa (Hawaii), Tenerife (Canary Islands) and Fogo (Cape Verdes), respectively. Whilst their findings help unlock the debate on the potential of giant collapses
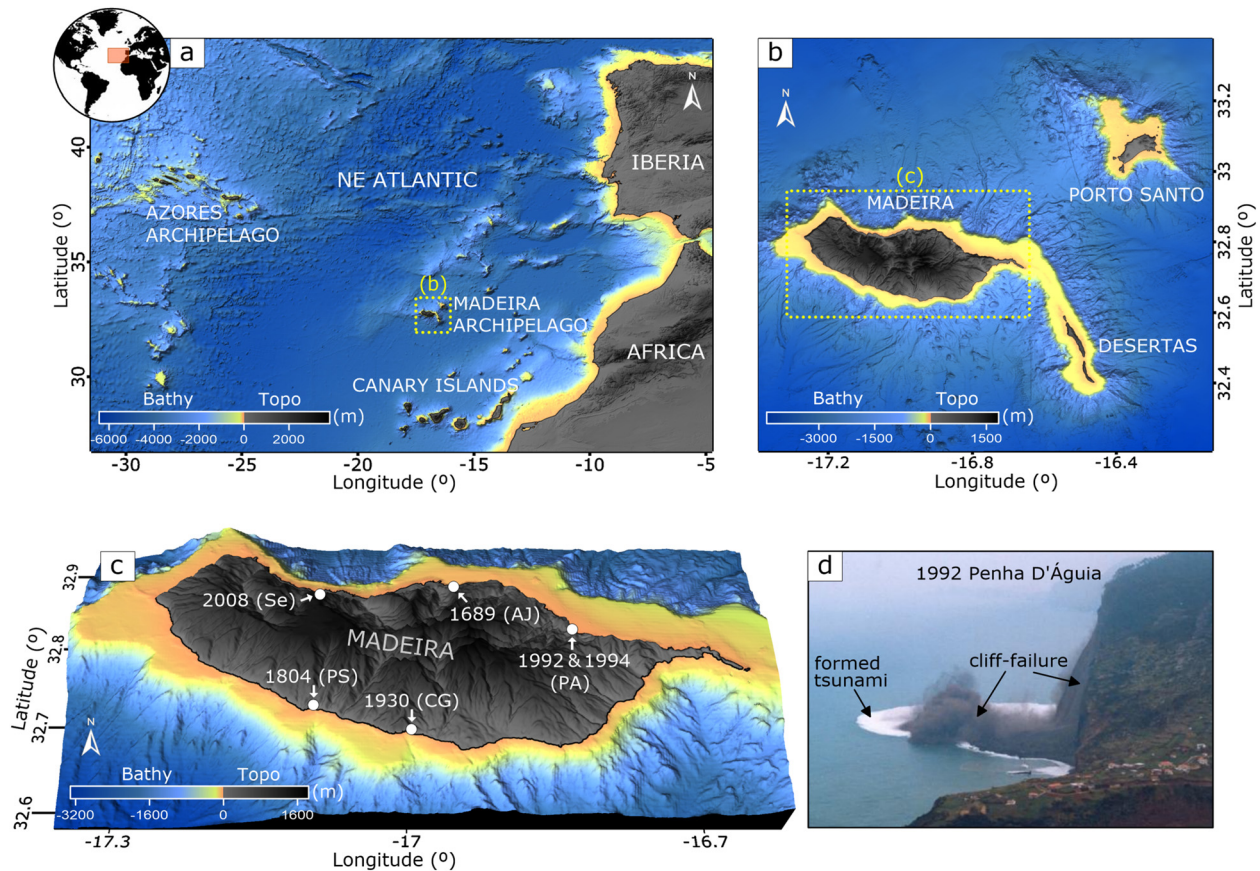
Fig. 1. (a) Overview of the NE Atlantic region where the main volcanic archipelagos stand; (b) Madeira Island within Madeira Archipelago, an island bound by high cliffs and prone to mass-wasting episodes; (c) Location of historical mass-wasting events occurred on the flanks of Madeira Island: Ponta do Sol (PS), Cabo Girão (CG), Penha D'Águia (PA), Arco S. Jorge (AJ), and Seixal (Se); (d) Photo of the 1992 Penha d'Água mass-wasting event and the tsunami it generated (source: http://aprenderamadeira.net/pedra-natural/). Bathymetric and topographic data used to produce the maps are from EMODNET (source: https://www.emodnet-bathymetry.eu/). (For interpretation of the colours in the figure(s), the reader is referred to the web version of this article.)

to generate extreme tsunamis, it is still hard to draw a general conclusion on the tsunamigenesis of all collapses in oceanic islands. This is so because the volume of the material involved during the failure is not the only parameter controlling the tsunamigenesis of flank collapses, but other factors (i.e., collapse process and dynamics) are highly influential.

A recent tsunami event involving a flank-collapse took place on December 22nd, 2018, following the eruption of the Anak Krakatau volcano in Indonesia (Paris et al., 2020; Grilli et al., 2021). The tsunami was generated when a sector of the island collapsed into the sea causing waves that struck along the rim of the Sunda Strait and resulted in 437 fatalities and many coastal houses heavily damaged (Putra et al., 2020). This event demonstrated the capability of point-sourced tsunamis to impact coastal zones located tens of kilometres from the source area and raised the limitation of the warning systems in forecasting such "silent" tsunamis (Omira and Ramalho, 2020). Moreover, it showed how urgent it is to improve our scientific understanding of collapse-triggered tsunamis and their mechanisms, in order to better assess the hazard potential posed by these events, as well as their frequency and consequences. Crucially, the Anak Krakatau event also raised the conscience that the debate is often too centred on the very low probability, but very high impact events associated to giant island lateral collapses, and that the consequences of tsunami events triggered by smaller but much more frequent cliff-failures are not properly being considered.

Coastal cliff-failures are a ubiquitous process in the evolution of cliff-bounded coastlines and there are reasons to believe that – with rising sea levels and an increase in coastal erosion as result

of global warming – they will become more frequent and consequently present a greater threat to coastal communities (Trenhaile, 2014). The issue of tsunamis triggered by coastal landslides is also especially relevant in the case of volcanic oceanic islands, as these are generally very prominent and unstable, and are particularly exposed to coastal erosion (Quartau et al., 2010; Ramalho et al., 2013; Melo et al., 2018; Huppert et al., 2020).

In few places of our planet the hazard posed by tsunamigenic cliff-failures is more acute than on the case of the Atlantic volcanic archipelagos, which are particularly prone to coastal mass-wasting (Quartau et al., 2010; Ramalho et al., 2013; Melo et al., 2018). Effectively, the Atlantic volcanic archipelagos of the Azores, Madeira, Canaries, Cape Verde and Tristan da Cunha feature some of the highest coastlines of any volcanic archipelagos in the world, with many of the islands being entirely cliff-bounded and exhibiting near-vertical cliffs that frequently attain heights of 300–800 m. Why the Atlantic volcanic islands generally feature such high (and unstable) coastlines rest on a fortuitous combination of factors: these islands are, by nature, extremely prominent volcanoes (on account of being built of alkalic volcanic sequences); they are subjected to low rates of volcanic growth and often to low subsidence rates, which facilitates coastal erosion (Ramalho et al., 2013; Quartau et al., 2018b); and – crucially – they are unprotected by coral reefs and are exposed to the extremely energetic wave regime of the Atlantic Ocean (Rusu and Onea, 2016). It is this combination of factors that led to the formation of high cliffs such as the ones at the western coast of Corvo (up to 720 m), the northern shore of São Jorge (up to 945 m), the western shore of Flores (up to

580 m), or the northern and western shores of Madeira (up to 500 m) (Fig. 1).

The instability of high coastal cliffs along the Atlantic islands is well attested by the presence of large coastal talus platforms – locally termed "fajãs", which result from the accumulation of land-slide debris at the foot of the cliff and the adjacent island shelf – and also by the numerous and well documented historical cliff-failure events, many of which were tsunamigenic (Rodrigues, 2005; Andrade et al., 2006; Ramalho et al., 2013; Melo et al., 2018). Madeira Island is a particularly good case study, since its histor-ical record is rich in eyewitness accounts of several mass-wasting events along its high coastal cliffs, namely in 1689, 1804, 1930, 1992, 1994 and 2008 CE (Rodrigues, 2005) (see Figs. 1c and 1d).

One of the better documented examples of a tsunamigenic cliff-failure in Madeira is the March 4th, 1930 event, which resulted from the failure of a sector of the Cabo Girão cliff, located in the southern shore (Fig. 1c). The collapsed material plunged into the sea and generated a local tsunami that propagated along Madeira´s southern coast and flooded the Vigário beach (Fig. 2 for location) at Câmara de Lobos, causing 19 casualties and 2 missing people (Ro-drigues, 2005). A more recent cliff-failure involving around 1.8x10⁶ m³ of material occurred in 1992 at Penha D´Água forming a small fajã with 300 m x 300 m. It generated a small tsunami that had no consequences at the neighbouring coastlines (Fig. 1d).

The aims of this study are twofold: (1) to contribute to a better understanding of the tsunami hazard posed by small-scale cliff-failure events; (2) to test and refine the application of state-of-the-art numerical modelling to generation, propagation and inundation of tsunamis triggered by small cliff-failures, here using the ex-cellent case study provided by the 1930 cliff-failure tsunami. To achieve these aims, we use detailed historical description, morpho-logical analysis, and evidence-calibrated numerical modelling of tsunami generation and propagation over a high-resolution digital bathymetric and topographic model. Our results are then explored to unlock, at least partially, the debate on the tsunamigenic poten-tial and hazard extent of small-scale events frequently occurring on the flanks of ocean volcanic islands.

2. Geological setting

Madeira is the largest and youngest island of Madeira Archipel-ago (Fig. 1b), with a volcanic history extending from >7 Ma to the Holocene (Geldmacher et al., 2000; Ramalho et al., 2015b). The island edifice is a prominent E-W elongated shield volcano that stands approximately 6 km above the surrounding seafloor, exhibiting an onshore area exceeding 700 km² and presently at-taining a maximum elevation of 1862 m above mean sea level, at Pico Ruivo. Despite its relatively young age, the island is deeply dissected by a dense river network, on account of torrential ero-sion driven by a high precipitation regime (Lira et al., 2013). The island was also the subject of large flank collapses – as demon-strated by a recent high-resolution multibeam bathymetric survey – which also contributed to increase the steepness of the volcanic edifice's flanks (Quartau et al., 2018a). The island shelf is relatively wide, particularly on the northern (windward) and southwestern sectors where it extends, respectively, up to 6 and 9 km offshore (Quartau et al., 2018a).

The coastline of Madeira is generally cliff-bounded, featuring numerous nearly vertical cliffs that frequently reach in excess of 300 m and up to nearly 600 m in elevation. Such cliffs are usually cut in thick, largely effusive sequences, which – on account of in-trinsic structural weakness derived by the prevalence of columnar jointing and alternation with more friable clinker and/or tephra layers – are prone to gravitational failure, triggering rockfalls, top-ples, debris avalanches and more rarely rotational landslides (Ro-drigues, 2005; Ramalho et al., 2013). These landslides are responsi-

ble for the formation of coastal talus platforms, which – notwith-standing their vulnerability to wave erosion – are a testimony to the relatively large volumes of collapsed material involved in these events.

Cabo Girão (32°39′23″N, 17°0′24″W) is a major landmark along the southern shore of the island, exhibiting a nearly verti-cal cliff of 589 m in elevation. The area has been the subject of numerous pre-historic and historic landslides, as it is discernible by the visible collapse scars on the cliff, and the talus accumula-tions of Fajã dos Padres (west of Cabo Girão proper) and Fajã dos Asnos (immediately below Cabo Girão), and Fajã das Bebras (east of Cabo Girão proper), which is the one that largely resulted from the March 4th, 1930 event (see Fig. 2). For the sake of simplicity, this event – occurred in the Pico do Rancho (Fig. 2c) – is referred hereinafter as the 1930 Cabo Girão landslide (CG in the modeling figures).

3. Data and methods

3.1. Retrieving the tsunami metrics from historical description

For a better understanding of what happened on March 4th, 1930 along the coast of Madeira Island, we scrutinized the doc-uments reporting the event and carefully analyzed the available descriptions to retrieve quantitative characteristics of the gener-ated tsunami and its impact. The newspapers "*Diário de Notícias*" n° *16678* (*DN16678*) and "*Diário da Madeira*" n° *5569* (*DM5569*), both of March 6th, 1930, provide a compilation of the best available in-formation on the Cabo Girão event. Additional descriptions of the cliff-failure and the resulting tsunami were also found in some recently published research works (Rodrigues, 2005; Baptista and Miranda, 2009). From these documents, we distinguished between information on the collapse mechanism, the tsunami generation, and the impact of the waves when reaching the coast.

3.1.1. The Cabo Girão cliff-failure and tsunami generation
The landslide occurred on March 4th, 1930, at 9:20 am, local time. The mass split as a whole from the cliff face of Pico do Ran-cho, which is ∼1.4 km to the ESE of Cabo Girão proper and is more than 350 m in height; it quickly disintegrated as it fell and the failure-involved material spread southwards. Simultaneously, a cloud made of dust was formed and then vanished westward, taken away by the strong breeze. The collapse led to the formation of a deposit (talus accumulation) that extended ∼500 m towards the south (∼200 m onshore and 300 m offshore) where it reached deep water and forming the landform that became known as Fajã das Bebras (Fig. 2). The involved material consisted of a mixture of rocks (basaltic lava flow and tuff blocks) and some loose soil.

According to eyewitnesses, "following the collapse, an enor-mous wave of several meters, looking like a cloud, was formed and moved fast towards the village" of Câmara de Lobos (Vigário beach and village Bay). At the same time, a strong sea swirling was observed in an opposing direction of the wave propagation.

3.1.2. Tsunami impact on Madeira coast
The Vigário beach was the coastal zone dramatically struck by the tsunami waves. At the moment of the sector collapse, women were washing clothes in a small lagoon of the Vigário stream mouth approximately 50 m away from the shoreline, while their children were playing nearby. Just beyond the stream mouth, sev-eral men were working, and on the opposite side, some fishermen were preparing two boats before going fishing. The warning sig-nal was given by the fishermen who first saw the incoming wave. The panic-stricken women ran to save their children, while others
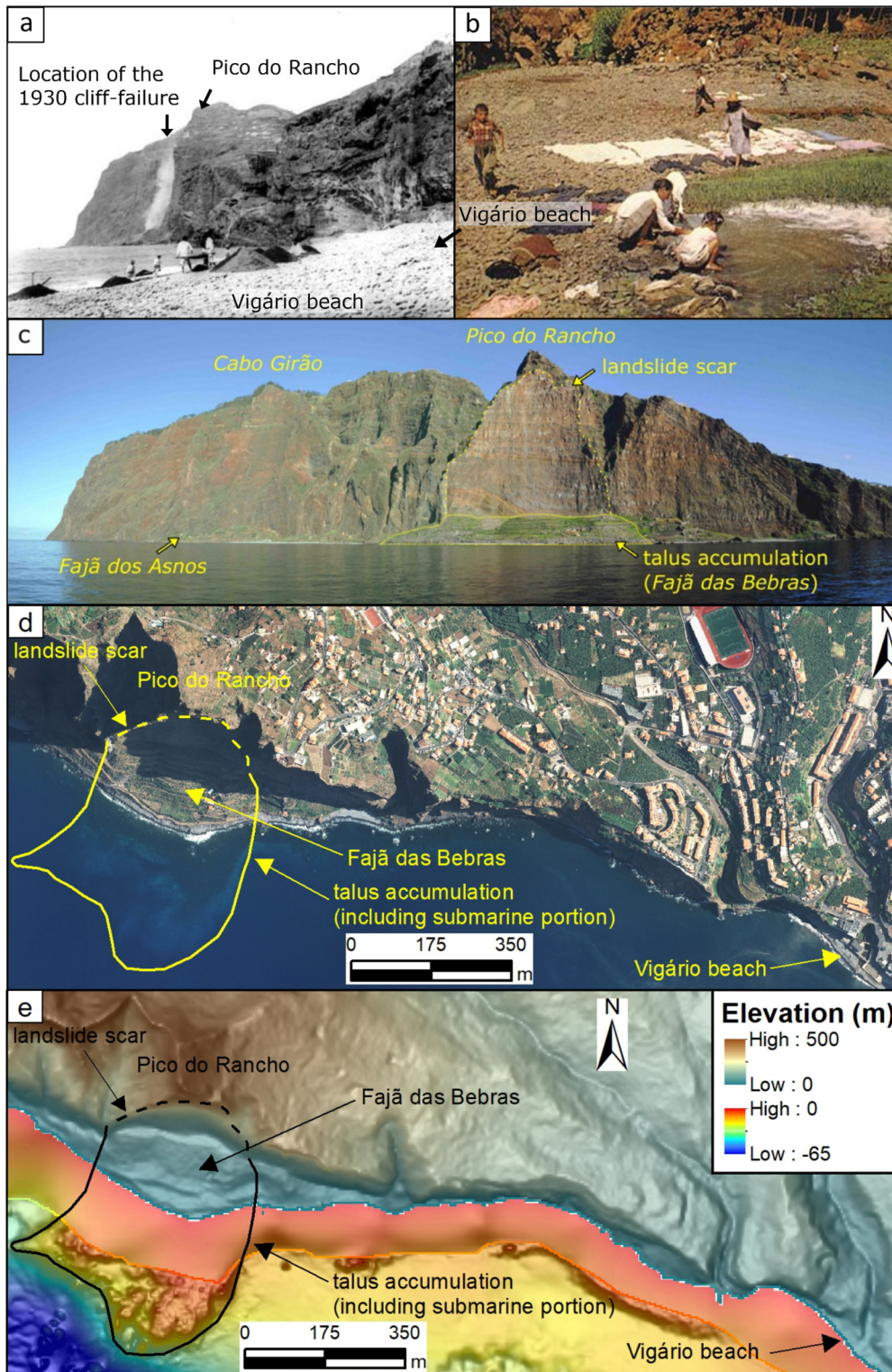
Fig. 2. Reconstruction of the cliff-failure of Cabo Girão in 1930 (a) Men extracting sand at the Vigário beach in the 30s of the 20th Century, about 100 m away from the failure site; (b) Women and children washing closes at the Vigário beach (photos are available from: http://www.concelhodecamaradelobos.com/dicionario/praia_vigario.html); (c) Panoramic photo (dated of 8th December 2004) of the cliff at Cabo Girão, showing the landslide scar at the cliff face of Pico do Rancho and the resulting talus accumulation that became known as Fajã das Bebras; the highest point of the collapse scar is at ~350 m in elevation; (d) Orthophoto of the area, showing the offshore extent of the talus accumulation, which is approximately 500 m from the cliff base; (e) The same image of (d) but showing the DEM's used in the reconstruction (see section 3.2 for details).

also tried to take the clothes they had spread on the pebbles. The river mouth in the Vigário beach was dramatically hit by the massive wave that dragged all who had no time to escape. When the wave receded, some women and children were seen among the foam and debris. From land, some men shouted for the women to grab the floating timber, but they couldn't save themselves and their children due to the strong water current.

At the bay of Câmara de Lobos, a fisherman lost two fishing crafts. Despite having climbed a ramp of 15 m height, the fisherman and his co-workers were still caught by the wave. The fish-
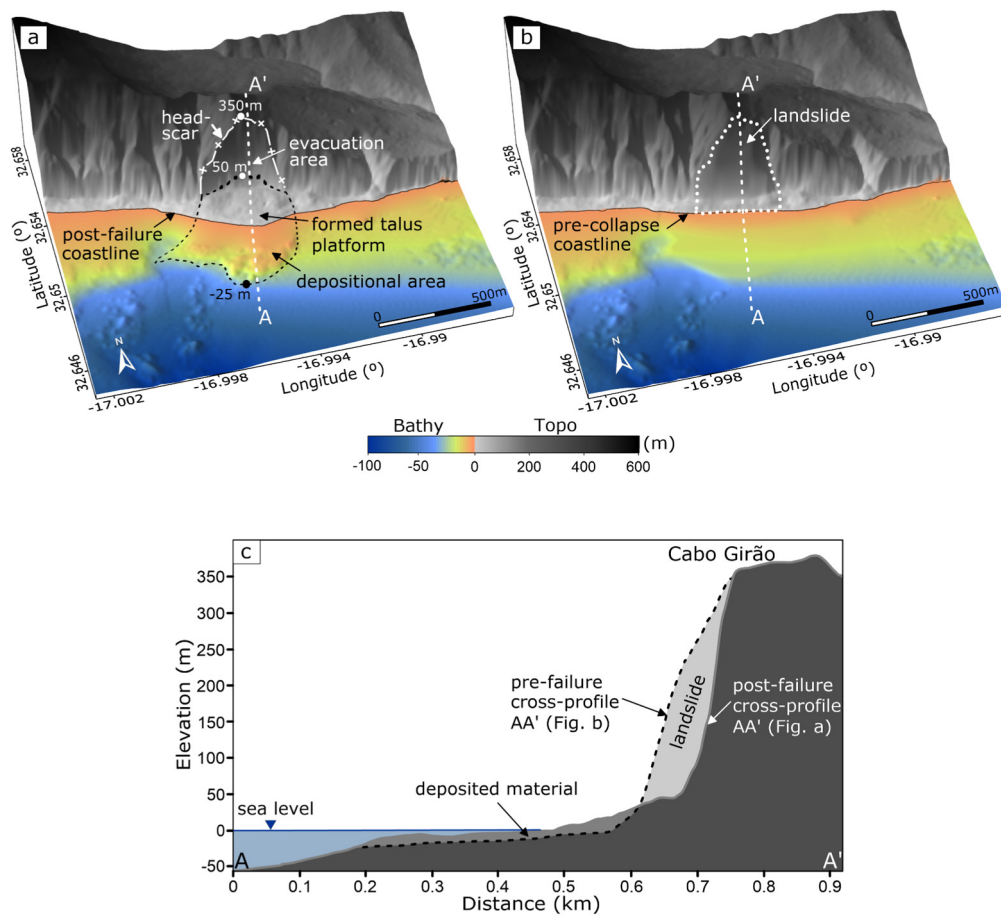
Fig. 3. Elevation model of Cabo Girão: a) Post-event (present day) bathymetric and topographic model including the main morphologic features of the Cabo Girão cliff-failure; b) Pre-event elevation model showing the reconstruction of the Cabo Girão landslide; c) cross-section of both pre- and post-failure elevation models of Cabo Girão cliff.

erman's house, where several families lived, was flooded through the window even though it is located at 15 m above sea level.

The Cabo Girão tsunami of 1930 resulted in 19 fatalities, 2 persons were reported missing and 6 were injured (Rodrigues, 2005). According to eyewitnesses, there was not a higher number of victims and loss of boats due to the ebbing tide and the rough sea that conditioned the regular fishermen activities the day of the event (DN16678). Reports indicated that approximatively 50 persons were working in the beach at the time of the event (Rodrigues, 2005).

3.2. Digital elevation model and landslide volume

We gathered the best available topographic and bathymetric data to build an accurate high-resolution digital elevation model (DEM) for the area of interest. We obtained, from Direção Regional do Ordenamento do Território e Ambiente of the Regional Government of Madeira, the coastal topography and ortophotos with respectively 5 m and 0.4 m horizontal resolution (Figs. 2d and 2e). Both data were based on vertical aerial photos acquired in 2007. The bathymetric data of nearshore water depths of 5-10 m down to a depth of 100 m was provided by the Portuguese Hydrographic Office with a resolution of 10 m (Fig. 2e). This bathymetry was acquired in 2002 with a multibeam pole-mounted Simrad EM3000 system (Instituto Hidrográfico, 2003). To fill the gap between the coastline and the high-resolution bathymetry we used the lower resolution EMODNET bathymetry (http://www.emodnet-bathymetry.eu) based on single beam data. Bathymetric data deeper than 100 m was also based on the EMODNET bathymetry. Through the compilation of these datasets we ob-

tained a 10 m resolution DEM that allowed a better representation of both bathymetric and topographic features of Cabo Girão and surrounding coastal areas, and consequently a detailed geomorphological analysis of this landslide.

For the sake of higher consistency, we combined two methods to infer the volume of the studied landslide. The first one, relied on the reconstruction of the pre-failure topography by the simple interpolation of slopes that are immediately adjacent to the collapse scar (e.g., Völker, 2010); the landslide volume was then obtained by subtracting the present-day topography from this interpolated topographic surface (Fig. 3). The other way determined the volume of the landslide deposit by comparison with the surrounding bathymetry without cliff-failures deposits. We used the orthophotos and the bathymetry to map the extent of the failed deposit (including subaerial and submarine parts) (Fig. 2e). Landslide volumes obtained by these methods are depicted in Table 1. As both volume estimate methods present uncertainties mainly associated with the accuracy of the topographic and bathymetric available data, the precise identification of the landslide scar and deposit extent, and the morphologic changes caused by erosion and deposition coastal processes, we averaged both volumes, obtaining 2.87 x 10^6 m^3 (Table 1).

Table 1
Volume estimate of the 1930 Cabo Girão landslide in Madeira Island.

Scar-derived volume (m^3)	Deposit-derived volume (m^3)	Averaged volume (m^3)
2.895 x 10^6	2.845 x 10^6	2.87 x 10^6

3.3. Tsunami numerical model

In this study we used a coupled depth-averaged two-layer model to simulate the mass-wasting movement and the tsunami it generates. The landslide is assumed as a viscoplastic deformable body and its downslope movement is simulated using the Bing-Claw model (Kim et al., 2019) that implements the Herschel-Bulkley rheology in a depth-integrated formulation. In the viscoplastic model, the landslide body is composed of two distinct zones: a shear deformable zone and a plug zone in which there is no deformation. BingClaw uses a finite volume numerical scheme to solve a system of a mass balance equation integrated over the entire flow depth and two separate momentum balance equations integrated over the depths of both the plug and shear zones.

For the numerical simulation of the Cabo Girão cliff-failure dynamics and the tsunami it generated, the densities of the landslide and water were set to 1500 kg m^{-3} and 1000 kg m^{-3}, respectively, and we tested various values of the yield stress (τ_y) to better mimic the deposited material. Parameterization of the landslide, scenarios tested and comparison of simulated deposits to observations are presented in Supplementary Material (S1). From these numerical tests, a yield stress of $\tau_y = 10$ kPa was used in the simulation of the landslide downslope movement as it allows a better reproduction of the morphological features, mainly the landslide thickness and runout, of the identified deposit.

The tsunami generation, propagation and inundation are simulated using the GeoClaw model (Berger et al., 2011) that solves the nonlinear shallow water (NLSW) equations in a finite volume scheme. GeoClaw assumes a hydrostatic pressure and captures the propagation of breaking waves, bottom drag, and dry-wet inundation using a moving boundary (shoreline) algorithm. The validity of the NLSW model to properly simulate the Cabo Girão tsunami was investigated by comparing numerical results of both dispersive and non-dispersive models, as landslide-tsunami tends to develop dispersive behaviour while propagating from the source area towards the coast. Here, synthetic tsunami waveforms using both NLSW (e.g., Berger et al., 2011) and Boussinesq-type (e.g., Kim et al., 2017) models are compared at different water depth locations. Details of this comparative assessment are presented in Supplementary Material (S2). The models show quite identical waveforms in the shallow water area (insular shelf) and very weak dispersive effects in the deep-water area (open ocean) and, therefore, non-dispersive tsunami model is considered applicable for our case study.

4. Results and discussion

4.1. Structural and morphological conditions favouring cliff-failures at oceanic islands

On volcanic islands, cliff instability and failure are particularly prevalent, as expected, along the windward or more exposed coasts of the volcanic edifices (if unprotected by coral reefs), where strong surf leads to faster wave erosion, cliff undercutting and a more effective erosion/transport of collapsed debris, leading to high and nearly vertical, often plunging seacliffs (Emery and Kuhn, 1982; Ramalho et al., 2013; Melo et al., 2018). The structure and composition of the cliffs – i.e., rock mass structure and strength – are also a critical factor in controlling cliff-failure and in determining the type (and volume) of landslides produced. For example, poorly unconsolidated pyroclastic sequences are friable and rapidly eroded but do not tend to generate tall cliffs and large landslides on account of their homogeneity and weakness. In contrast, the tallest cliffs and largest events of cliff-failure are generally associated with gently-dipping, largely effusive se-

quences, where simultaneously the hardness of materials leads to a higher resistance to erosion, but the heterogeneity of the materials and the pervasive columnar jointing of the lava flows promotes larger, vertically-propagating (from toe to crest) and less frequent failures, thus leading to a more episodic and threshold-driven failure behaviour (Ramalho et al., 2013; Melo et al., 2018). In these sequences, coastal retreat is chiefly the net result of a continuous horizontal erosive component provided by mechanical wave erosion and an episodic vertical erosive component provided by episodic mass wasting (Ramalho et al., 2013). In this respect, the cliffs of Cabo Girão are no exception and in fact constitute a good case study of how largely effusive (or mixed lava flow/pyroclastic) sequences are prone to develop tall nearly vertical cliffs and are subjected to episodic collapse.

In what concerns the triggering mechanisms for large cliff-failures, the situation is more complex. The stochastic behaviour of cliff-failures suggests that several mechanisms may contribute – and interact – to trigger failure events. There is no doubt that mechanic wave erosion and cliff undercutting/toe notching is a determining factor in creating the conditions for failure, but what triggers the actual event is more enigmatic. Examples of large cliff-failures during or immediately after stormy conditions – when high rainfall and strong surf contribute to the rapid escalating of forces and the surpassing of threshold conditions – abound (e.g., Melo et al., 2018). It has been recognized that high rainfall followed by increased groundwater recharge may cause the gravitational loading and increased pore water pressure, resulting in reduced shear strengths that may result in failure (Stephenson, 2014; Dietze et al., 2020). The increased pounding of storm surf on plunging cliffs results in vibrations that may equally induce failure; in a similar fashion, earthquakes have been recognized as triggering significant coastal failures, as it happens in the tectonically active Azores Archipelago. Significant failures, however, were also registered during periods of fair weather or seismic quiescence, as it is the case of the 1930 Cabo Girão and the 1992 Penha d'Águia landslides in Madeira. The triggering mechanism of large coastal cliff-failures is thus complex, non-linear and very difficult to predict, possibly resulting from a combination of factors which include toe notching, progressive fracture and facilitated connectivity from toe to crest, terrestrial controls on rock moisture, amongst other marine and subaerially controlled factors (Rosser et al., 2013). Given these considerations, the triggering mechanisms for the 1930 Cabo Girão landslide remain unknown, but a lesson to retain is that such events may happen without warning.

4.2. Pre-failure topography and tsunamigenesis of the Cabo Girão cliff

Analysis of Figs. 2 and 3 shows that the failure is initiated at an elevation of 350 m marking the top of the rim of the head-scar. The depositional area covers 1.7 x 10^5 m^2 and is bounded at the top by the foot of the head-scar located at 50 m elevation and at the bottom by the foot of the landslide, located at 25 m of water depth (Fig. 3a). The landslide runout is up to 500 m with material deposited both on- and offshore (Figs. 2 and 3).

In agreement with eyewitness observations of the 1930 event, our simulations show that the failure of Cabo Girão steep cliff into the sea, involving a volume of 2.87 x 10^6 m^3, leads to the generation of a tsunami. Fig. 4 depicts the tsunami generation process, including the temporal evolution of the landslide mass movement (Figs. 4a to 4c) and the ensuing wave formation (Figs. 4d to 4f). At t = 0 s the cliff-failure is initiated, and the evacuated material starts moving downslope (Figs. 4a and 4d). It immediately plunges into the sea (Fig. 4b) and perturbs the nearshore water column leading to the formation of a large wave of about 8 m in height (Figs. 4e). We find that the removed material moves fast
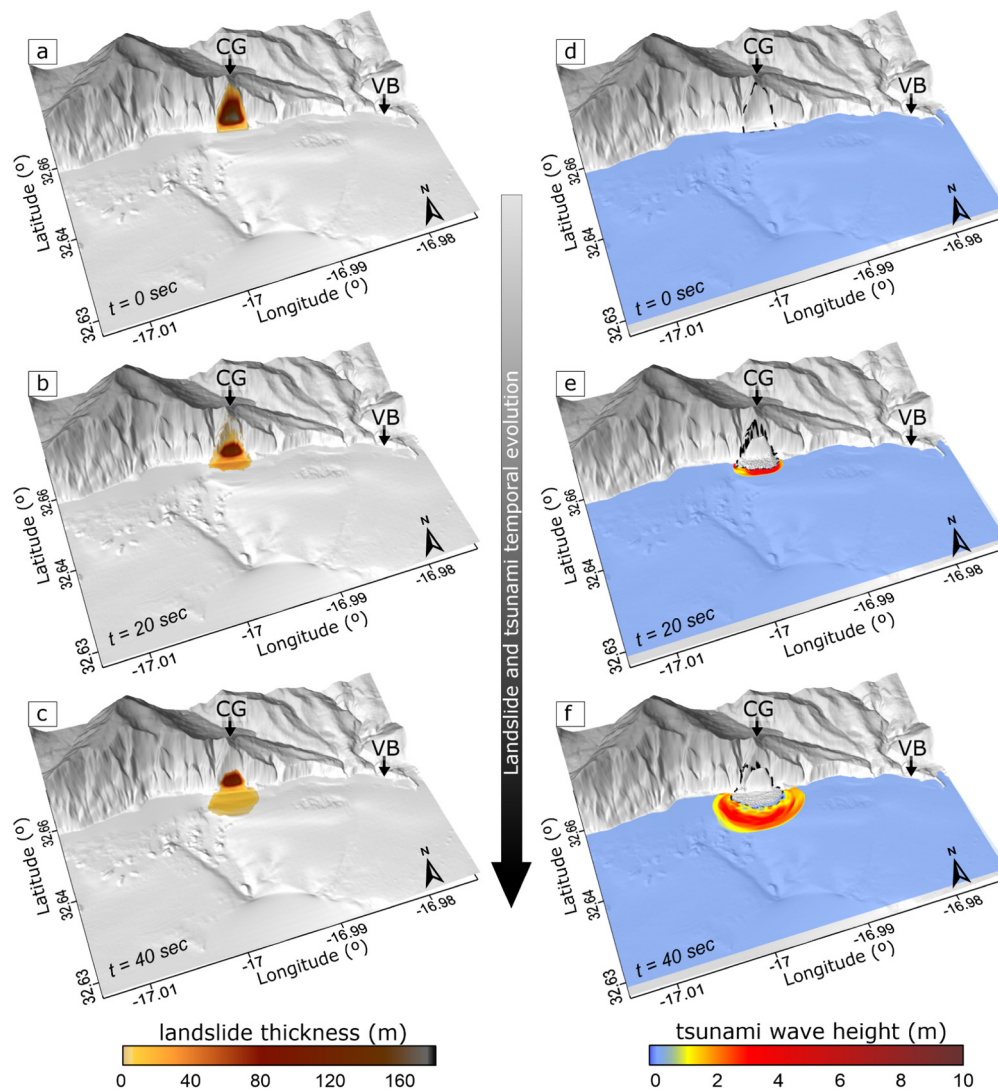
Fig. 4. Simulations of Cabo Girão cliff-failure dynamics and tsunami generation: a) to c) Snapshots of the downslope mass failure movement; d) to f) Snapshots of tsunami generation, black dashed contours mark the landslide limits. CG, Cabo Girão; and VB, Vigário Beach.

down the steep cliff slope of ∼78°. It then encounters the shallow submarine platform with a gentle slope (∼2.5°) that slows down its movement. The landslide quickly reaches the steady state after 40 s of movement, exhibiting a runout distance up to 500 m (Fig. 4c), reproducing fairly the offshore deposit extension and geometry. At this stage, the resulting tsunami wave has a height of ∼6 m (Fig. 4f), in general agreement with eyewitness accounts. Our numerical results also show that a significant amount of the collapsed material is deposited on- and near-shore (Figs. 4c and 4f), in agreement with available eyewitness descriptions and morphological observations. This leads to a noticeable change in the shoreline configuration caused by the formation of a coastal talus-platform, which is also in agreement with the formation of what the locals named Fajã das Bebras, a landform that still exists albeit some marine erosion and coastal retreat since its formation (Figs. 2 and 3). Given these results, which match very well both the contemporaneous eyewitness accounts and the present-day morphological characteristics of the collapse scar and deposits, we are very confident that our numerical simulations reasonably reproduce the 1930 event and its effects, albeit some differences in the detail of matching the offshore deposit (see Supplementary Material S1) that we assume has no significant impact on the main results.

4.3. Tsunami propagation and hazard extent of the Cabo Girão event

Unlike earthquake-triggered tsunamis that are generated by seafloor displacement typically in the open ocean (i.e., deep water) and then travel towards the coast, the Cabo Girão was a small- to moderate-sized point-sourced tsunami that was generated at the island coast and shelf, by a largely subaerial landslide falling in shallow water, which then propagated towards the open ocean and surrounding coastal areas. The tsunami energy pattern (in terms of max. wave heights) and inundation (in terms of max. flow depths) presented in Fig. 5 provide useful insights into the hazard posed by the Cabo Girão cliff-failure tsunami. At the local scale, our simulations show that the tsunami reached the nearest coastal areas immediately (few minutes) after the cliff-failure (Fig. 5a). Here, at a first order, the simulated tsunami height is maximum (5-8 m, Fig. 5a) in the direction of the landslide movement. It then significantly decreases when propagating towards the deep water (1-2 m, Fig. 5a). Critically, our numerical simulations emphasize that the tsunami waves undergo a significant amplification over the inner part of the shelf, being maximum in both the western and eastern directions of the failure (arrows in Fig. 5a), rather than in the frontal area of the landslide, i.e., the shallow shelf guides the larger tsunami waves towards the nearest coasts. Among the affected coastal areas, the highest tsunami waves propagate towards
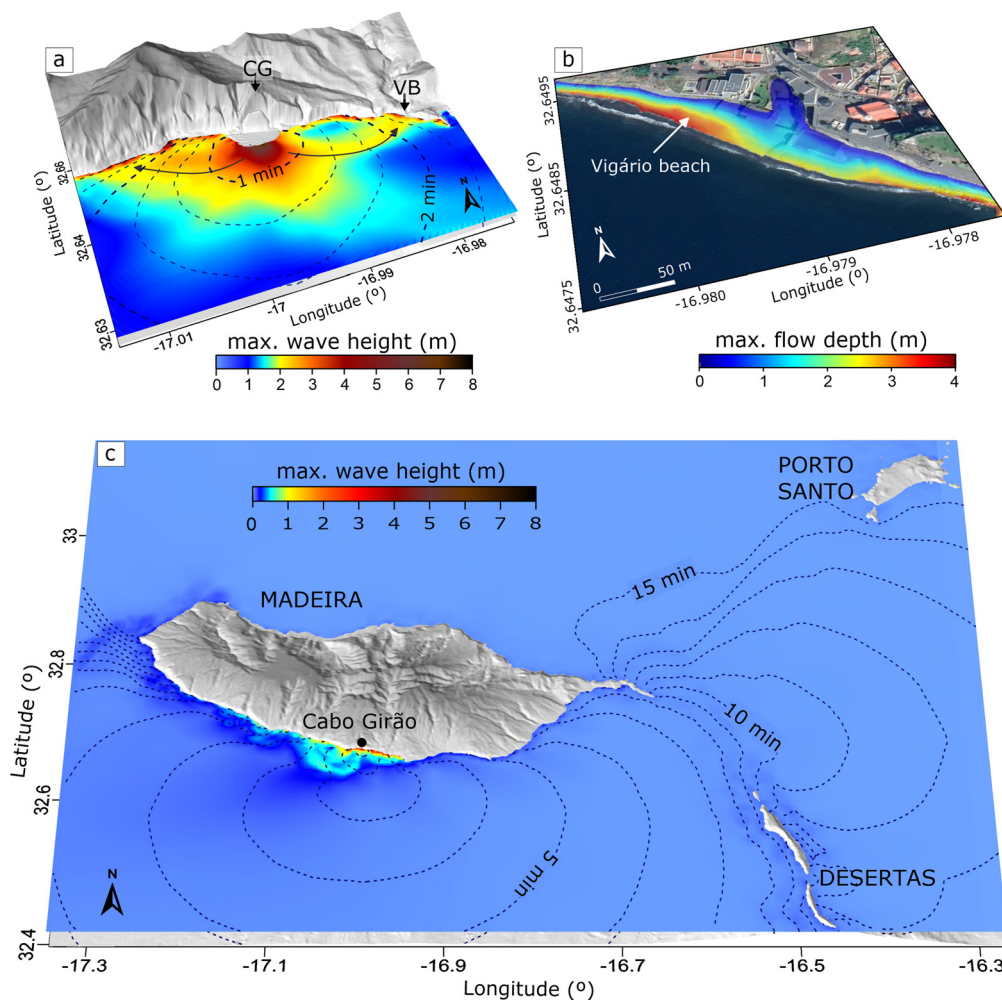
Fig. 5. Cabo Girão point-sourced tsunami hazard extent: a) local-scale tsunami maximum wave height and travel time (contours each 20 s); b) tsunami inundation at Vigário beach; c) regional-scale tsunami maximum wave height and travel time (contours each 1 min).

the Vigário beach, where effectively most tsunami victims were reported. Here, the incident waves are as high as 4-5 m (Fig. 5a). Our simulations suggest that these waves caused the inundation of the entire Vigário beach with an estimated maximum flow depth of 4 m, an inundation distance up to 110 m, and a maximum runup height of 12 m (Fig. 5b). Whilst the simulated runup height at Vigário beach is comparable to that from the tsunami impact description (15 m, see Sect. 3.1.2), our numerical model slightly underestimates the maximum inundation distance. We believe that the use of the present-day coastal DEM for both the collapse area – which probably underestimates the landslide runout and volume – and the impacted coast (Vigário beach) influences the modelling results. The lack of detailed bathymetry on the shallowest areas of the shelf (technically very challenging to survey) may also have contributed to some inconsistency between the modelled and described hazard metrics.

At the regional scale, the tsunami energy seems to undergo a significant dissipation while the waves travel away from the source area and get around Madeira's coast (Fig. 5c). According to our simulations, the tsunami arrived at the north-western coast of Madeira after 15 min of propagation with heights less than 0.2 m (Fig. 5c). Our results also show that the Desertas islands, located at ∼18.5 km to the SE of Madeira, are only reached by a negligible tsunami wave (∼5 cm) within 10 min, whilst no tsunami is observed at Porto Santo island, located at ∼39.5 km to the NE of Madeira (Fig. 5c). These results confirm that the 1930 Cabo Girão tsunami

was a point-source event of high local impact and very limited regional hazard extent, in agreement with eyewitness accounts.

Crucially, given that our numerical simulations were able to reproduce the historical event and its effects with a high degree of accuracy (notwithstanding some uncertainty in some parameters), this study demonstrates the utility of such approach to the investigation of the hazard posed by tsunamis triggered by the gravitational failure of tall plunging cliffs, thus opening an avenue for more detailed hazard studies. Moreover, this study emphasizes how state-of-the-art numerical modelling – made possible by high-resolution topographic/hydrographic datasets – may be used to better explore the relative vulnerability of coastlines to tsunamis triggered by near-field cliff-failures, with implications in terms of coastal engineering (e.g., in the design of tsunami-resilient coastal structures), territorial managements of coastal zones, civil protection, insurance policies, and disaster risk reduction.

4.4. Tsunamigenesis of small-scale mass-wasting events in volcanic islands

The tsunamigenic potential of mass-wasting events has been recognized over the last 2-3 decades, but the failure mechanisms and dynamics leading to the formation of tsunamis, when the evacuated material plunges into the sea and moves downslope, are still poorly understood (Paris et al., 2018 and references therein). The lack of knowledge in this field primarily lies on the absence of direct and instrumental observations. Alternatively, the volume

of the failure material, often inferred from mass transport deposits offshore and/or collapse scar onshore, is commonly considered as the main indicator of the tsunamigenesis of mass-wasting events. This applies to pre-historic catastrophic flank collapses involving tens to hundreds of cubic kilometres that were extensively studied in the Pacific Ocean (e.g., Hawaii, Moore et al., 1995; McMurtry et al., 2004), Atlantic Ocean (e.g., Canary Islands and Cape Verde, Ward and Day, 2001; Paris et al., 2017; Barrett et al., 2020) and Indian Ocean (e.g., Krakatau, Maeno and Imamura, 2011) to establish the link between their volume and the generation of "megatsunamis". However, recent events such as Stromboli in December 2002 (Tinti et al., 2006) and Anak Krakatau in December 2018 (Paris et al., 2020; Grilli et al., 2021) have evidenced that smallscale collapses (< 0.5 km^3) are also capable of causing deadly tsunamis. Smaller scale events such as cliff-failures of the tall coastlines of volcanic islands in the NE Atlantic are relatively frequent (Cabral, 2009; Melo et al., 2018). These produce coastlines that are frequently bordered by these low-lying platforms where a non-negligible part of the population of the islands live, have access to sea, or grow their crops. For instance, a similar event to the one studied here, occurred at Flores Island in the Azores; in 1857, a cliff-failure produced the fajã of Quebrada Nova with $\sim$0.009 km^3, triggering a tsunami with a runup of 5-7 m in Flores and the neighbouring Corvo Island, just $\sim$22 km apart. This tsunami injured $\sim$100 people, and caused 10 deaths in the two islands, all along the low-lying fajãs of these islands (Cabral, 2009). A more recent example is the November 14th, 2020 cliff-failure at Gomera Island -Canary Islands- that caused a relatively small tsunami with wave heights in the range of 0.5 m reaching a village located 200 m away from the source (Galindo et al., 2021).

With these recent events in mind, there has been an increasing focus on the failure mechanism and dynamics of landslides as factors influencing the tsunami formation and hazard extent (Omira and Ramalho, 2020; Zengaffinen et al., 2020). A major source of uncertainty in the failure mechanism of flank sectors concerns their occurrence as a single or a sequence of multiple events, either in close succession or at a protracted timescale. Although insights into this feature can be inferred from detailed analyses of high-resolution post-event bathymetry, seismic reflection profiles and/or seismic stations records of mass movement, the availability of such data remains scare. Understanding the dynamics of the collapse requires, on the other hand, real-time monitoring of the failure occurrence and its movement and/or accurate numerical modelling using in-situ determined physical and geotechnical properties of the material involved.

To our knowledge, less studied is the influence of the island coastal morphology in the tsunamigenic potential of sector collapses. In what concerns tsunamis triggered by smaller coastal cliff-failures, the island morphology – onshore and offshore – is a particularly determining factor in the dynamics of collapsed sectors and, therefore, on their tsunamigenesis and hazard extent. Such an effect is explored here through developing a conceptional tsunami formation model for two common coastal morphologies of ocean volcanic islands (Fig. 6).

Most oceanic volcanic islands exhibit insular shelves (i.e., shallow submarine platforms surrounding the islands), formed mostly by the combined effects of wave erosion of volcanic inactive coastlines, glacio-eustatic oscillations, and subsidence/uplift (Quartau et al., 2010, 2018b; Ramalho et al., 2013). The presence of insular shelves conditions the dynamics of collapse emplacement and consequently of tsunami generation (Fig. 6, right panel). When cliffs fail into the sea the collapsed material encounters a shallow submarine platform with a gentle slope that decelerates its flow (Figs. 6b and 6c, right panel). This often leads to the deposition of an amount of the evacuated material within the shoreline resulting in an alteration of the coastal morphology and creation of

a Fajã (Fig. 6d, right panel). This particular process influences the tsunami generation as only a part of the collapsed material, i.e., effective landslide volume, continues moving over the shelf gentle slope displacing the water body and generating a solitary-like initial wave (Figs. 6b and 6c, right panel). Moreover, the generated wave will then propagate in the relatively shallow waters of the shelf – particularly on the wider shelves of older islands – experiencing dissipation towards the offshore but – critically – amplification along the shallower near-shore areas, causing significant damage to near-field shorelines.

In contrast, on islands subjected to: (a) vigorous active volcanism, where magma-supply rates result in accumulation rates at coastlines that exceed erosion rates, the progradation of coastal lava deltas is dominant (Mitchell et al., 2008; Quartau et al., 2015); (b) recent flank collapses and/or lava delta gravitational slumps (on coasts subjected to rapid volcanic progradation, Sansone and Smith, 2006; Bosman et al., 2014); and (c) calm waters and very low erosion rates, island shelves are not able to develop, resulting in steep submarine slopes down to the abyssal plains (Ramalho et al., 2013). On such coastlines (Fig. 6), the dynamics of the collapse is marked by large runout distances, resulting from a fast movement over a steep slope (Fig. 6, left panel). As the collapse material moves downslope, it continuously pumps energy into the water column leading to the formation of an initial N-wave with a large depression (Figs. 6b and 6c, left panel). This is also the case when large-scale island lateral collapses occur, which generally involve both the subaerial and the submarine parts of whole island flanks; in this case the existence or inexistence of the island shelf will not affect tsunamigenesis in any significant way as the collapse also includes the shelf.

In general, the ability of a tsunami to travel away from its source region relies on whether the generated wave contains enough energy to allow such an extent. For flank collapse-induced tsunamis the generation phase is completed when the sliding material reaches the steady state. At this stage, the energy of the formed wave is composed of a potential energy E_p derived from the elevation of the free sea surface (η) ($E_p = \frac{1}{2} \int \rho g \eta^2 ds$, where ρ is the density of water, g is the acceleration due to gravity, and ds is the infinitesimal area element (Dutykh and Dias, 2009)) and a kinetic energy E_k estimated from the wave speed (u) ($E_k = \frac{1}{2} \int \rho H u^2 ds$, where ρ is the density of water, H the total water depth, and ds is the infinitesimal area element (Dutykh and Dias, 2009)). In volcanic islands exhibiting insular shelves, the formed tsunami wave often loses a part of its E_p as the amount of the evacuated material involved in the formation of the fajã does not contribute to the disturbance of the nearshore water body. This process results in forming an initial wave (solitary-like) of relatively short wavelength and, therefore, of reduced E_p. A similar effect was revealed for tsunamis generated by large earthquakes on nearshore subduction zones, where a part of the co-seismic deformation occurs onshore and does not contribute to the wave generation (Omira et al., 2016b). Moreover, the presence of the insular shelf affects the E_k of the tsunami at both stages of generation and propagation. It decelerates the movement of both landslide and formed wave and channels the tsunami energy. The latter occurs due to the important exchange of E_k and E_p of waves trapped in the shelf, resulting in a locally focused tsunami impact while only waves with small heights escape the shallow area and propagate away from the source.

In clear contrast to events taking place on islands with surrounding shelves, both the loss of an amount of E_p of the triggered wave due to the formation of onshore morphologic features and the shelf channelling of tsunami energy do not occur on oceanic islands without shelves (Figs. 6b and 6c, left panel). Here, the formed N-wave contains more energy pumped by the continuous and fast downslope movement of the evacuated material. Such
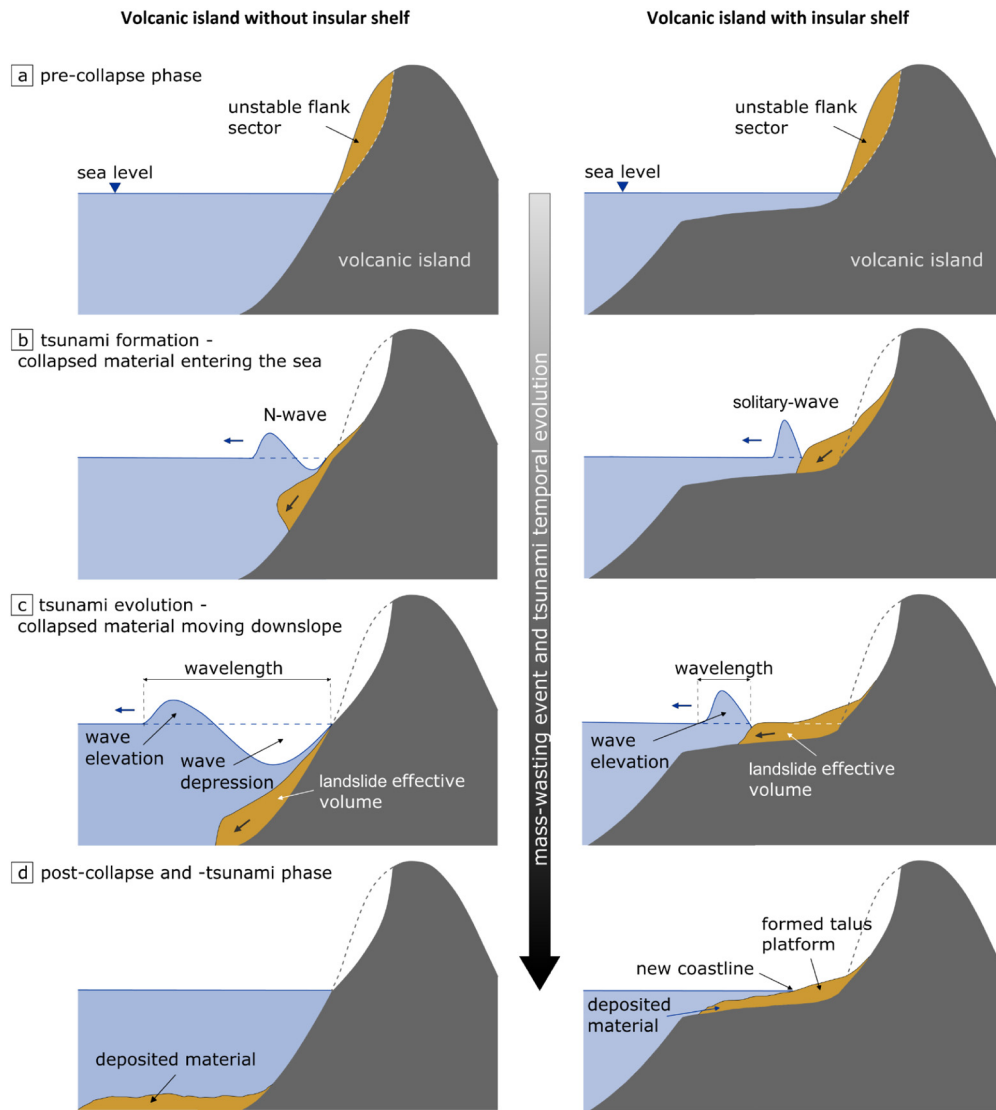
Fig. 6. Morphology-based conceptional model of tsunamigenic potential of small-scale mass-wasting events on volcanic islands flanks.

generated tsunamis have more potential to travel away from the source area without remaining trapped in the shelf and dissipating energy in such a shallow morphologic feature. The 1930 Madeira Island, studied here, and the 2018 Anak Krakatau tsunami events are prime opposite examples supporting our conceptional model on the influence of the island submarine morphology on the tsunamigenesis and hazard extent of mass-wasting-triggered tsunamis. While the 1930 cliff-failure caused a solitary-type wave (see wave profiles in the Supplementary Material S3, Fig. S3.1) leading to a very limited regional hazard extent (Fig. 5c), the 2018 Anak Krakatau collapse - regardless of its volume and failure mechanism that also involved a submarine part - occurred in a part of the island not surrounded by a shelf, triggering a relatively long N-wave tsunami (see wave profiles in the Supplementary Material S3, Fig. S3.2) that caused a regional impact on the Sunda Strait coasts (Putra et al., 2020).

Consequently, for the same volume involved in a costal cliff-failure event, the resulting wave characteristics will differ between the distinct islands' morphologies (Fig. 6), which could eventually lead to different tsunami hazard extents. This conceptual model should thus be considered when investigating the tsunamigenic hazard extent of small-scale coastal landslides.

5. Conclusions

This work contributes to unlock the debate on the tsunamigenic potential and hazard extent induced by small-scale mass-wasting events in oceanic volcanic islands. It benefits from the study of the prime example of Madeira -an island highly vulnerable to small mass-wasting and tsunami generation- and presents the first numerical investigation of the 1930 Cabo Girão cliff-failure and its ensuing tsunami. The numerical modelling results fairly reproduce the available description of the tsunami generation and coastal inundation, critically demonstrating the applicability of this approach to coastal vulnerability studies and for disaster risk reduction. They also demonstrate the high local and limited regional impact of such a point-source tsunami event. The detailed study of the 1930 event helps proposing a conceptional model that allows a better understanding of both the tsunamigenesis and tsunami hazard induced by small-scale mass-wasting events occurring on distinct islands with distinct submarine morphological settings. The morphology-based model reveals a localized tsunami hazard for islands exhibiting insular shelves and greater potential of regional to far-field tsunami impacts for islands without surrounding shelves. A proof of concept of the proposed model requires, how-

ever, extensive numerical testing of different coastal configurations and landslide volumes. Regardless of the island morphology, implementing forecast capabilities for such "silent" tsunami events remains an open challenge due to the absence of real-time monitoring and the short travel time of the waves to the threatened coasts.

CRediT authorship contribution statement

R. Omira: conceptualization, original draft, numerical modeling, figures preparation, results interpretation & discussion; **M. A. Baptista:** historical data, review & editing; **R. Quartau:** data provision, elevation model, writing, review & editing, **R. S. Ramalho:** photos provision and interpretation, writing, review & editing; **J. Kim:** numerical modeling, interpretation, review & editing; **I. Ramalho:** figures preparation, review & editing; **A. Rodrigues:** data provision, review & editing.

Declaration of competing interest

The authors declare that they have no known competing financial interests or personal relationships that could influence the work presented in this paper.

Acknowledgements

Appendix A. Supplementary material

Supplementary material related to this article can be found online at https://doi.org/10.1016/j.epsl.2021.117333.

References

Andrade, C., Borges, P., Freitas, M.C., 2006. Historical tsunami in the Azores archipelago (Portugal). J. Volcanol. Geotherm. Res. 156 (1–2), 172–185. https://doi.org/10.1016/j.jvolgeores.2006.03.014.

Baptista, M.A., Miranda, J.M., 2009. Revision of the Portuguese catalog of tsunamis. Nat. Hazards Earth Syst. Sci. 9 (1), 25–42. https://doi.org/10.5194/nhess-9-25-2009.

Barrett, R., Lebas, E., Ramalho, R., Klaucke, I., Kutterolf, S., Klügel, A., Lindhorst, K., Gross, F., Krastel, S., 2020. Revisiting the tsunamigenic volcanic flank collapse of Fogo Island in the Cape Verdes, offshore West Africa. Geol. Soc. (Lond.) Spec. Publ. 500 (1), 13–26. https://doi.org/10.1144/SP500-2019-187.

Berger, M.J., George, D.L., LeVeque, R.J., Mandli, K.T., 2011. The GeoClaw software for depth-averaged flows with adaptive refinement. Adv. Water Resour. 34 (9), 1195–1206. https://doi.org/10.1016/j.advwatres.2011.02.016.

Bosman, A., Casalbore, D., Romagnoli, C., Chiocci, F., 2014. Formation of an 'a'ā lava delta: insights from time-lapse multibeam observations and direct observations during the Stromboli 2007 eruption. Bull. Volcanol. 76, 1–12. https://doi.org/10.1007/s00445-014-0838-2.

Cabral, N., 2009. Análise do perigo de tsunamis nos Açores/Hazard assessment of tsunamis in the Azores. PhD thesis. Universidade dos Açores: Ponta Delgada. p. 170.

Carracedo, J.C., 1999. Growth, structure, instability and collapse of Canarian volcanoes and comparisons with Hawaiian volcanoes. J. Volcanol. Geotherm. Res. 94 (1–4), 1–19. https://doi.org/10.1016/S0377-0273(99)00095-5.

Carracedo, J.C., 1996. A simple model for the genesis of large gravitational landslide hazards in the Canary Islands. Geol. Soc. (Lond.) Spec. Publ. 110 (1), 125–135. https://doi.org/10.1144/GSL.SP.1996.110.01.10.

Day, S.J., Da Silva, S.H., Fonseca, J.F.B.D., 1999. A past giant lateral collapse and present-day flank instability of Fogo, Cape Verde Islands. J. Volcanol. Geotherm. Res. 94 (1–4), 191–218. https://doi.org/10.1016/S0377-0273(99)00103-1.

Dietze, M., Cook, K.L., Illien, L., Rach, O., Puffpaff, S., Stodian, I., Hovius, N., 2020. Impact of nested moisture cycles on coastal chalk cliff failure revealed by multi seasonal seismic and topographic surveys. J. Geophys. Res., Earth Surf. 125, e2019JF005487. https://doi.org/10.1029/2019JF005487.

Dutykh, D., Dias, F., 2009. Energy of tsunami waves generated by bottom motion. Proc. R. Soc. A 465, 725–744. https://doi.org/10.1098/rspa.2008.0332.

Emery, K.O., Kuhn, G.G., 1982. Sea cliffs: their processes, profiles, and classification. Geol. Soc. Am. Bull. 93 (7), 644–654. https://doi.org/10.1130/0016-7606(1982)93<644:SCTPPA>2.0.CO;2.

Geldmacher, J., van den Bogaard, P., Hoernle, K., Schmincke, H.-U., 2000. The 40Ar/39Ar age dating of the Madeira archipelago and hotspot track (eastern North Atlantic). Geochem. Geophys. Geosyst. 1, 1–26. https://doi.org/10.1029/1999GC000018.

Galindo, I., Romero, C., Martín-González, E., Vegas, J., Sánchez, N., 2021. A review on historical tsunamis in the Canary Islands: implications for tsunami risk reduction. Geosci. 11, 222. https://doi.org/10.3390/geosciences11050222.

Grilli, S.T., Zhang, C., Kirby, J.T., Grilli, A.R., Tappin, D.R., Watt, S.F.L., Hunt, J.E., Novellino, A., Engwell, S., Nurshal, M.E.M., Abdurrachman, M., 2021. Modeling of the Dec. 22nd 2018 Anak Krakatau volcano lateral collapse and tsunami based on recent field surveys: comparison with observed tsunami impact. Mar. Geol. 440, 106566. https://doi.org/10.1016/j.margeo.2021.106566.

Huppert, K.L., Perron, J.T., Ashton, A.D., 2020. The influence of wave power on bedrock sea-cliff erosion in the Hawaiian Islands. Geology 48, 499–503. https://doi.org/10.1130/G47113.1.

Instituto Hidrográfico, 2003. Dinâmica Sedimentar da costa sul da ilha da Madeira. REL.TF.GM.02/03. Instituto Hidrográfico, Lisboa, Portugal. p. 161.

Kim, J., Løvholt, F., Issler, D., Forsberg, C.F., 2019. Landslide material control on tsunami genesis—the Storegga Slide and tsunami (8,100 years BP). J. Geophys. Res., Oceans 124 (6), 3607–3627. https://doi.org/10.1029/2018JC014893.

Kim, J., Pedersen, G.K., Løvholt, F., LeVeque, R.J., 2017. A Boussinesq type extension of the GeoClaw model-a study of wave breaking phenomena applying dispersive long wave models. Coast. Eng. 122, 75–86. https://doi.org/10.1016/j.coastaleng.2017.01.005.

Lira, C., Lousada, M., Falcão, A.P., Gonçalves, A.B., Heleno, S., Matias, M., Pereira, M.J., Pina, P., Sousa, A.J., Oliveira, R., Almeida, A.B., 2013. The 20 February 2010 Madeira Island flash-floods: VHR satellite imagery processing in support of landslide inventory and sediment budget assessment. Nat. Hazards Earth Syst. Sci. 13, 709–719. https://doi.org/10.5194/nhess-13-709-2013.

Maeno, F., Imamura, F., 2011. Tsunami generation by a rapid entrance of pyroclastic flow into the sea during the 1883 Krakatau eruption, Indonesia. J. Geophys. Res., Solid Earth 116, B09205. https://doi.org/10.1029/2011JB008253.

McGuire, W.J., 2006. Lateral collapse and tsunamigenic potential of marine volcanoes. Geol. Soc. (Lond.) Spec. Publ. 269 (1), 121–140. https://doi.org/10.1144/GSL.SP.2006.269.01.08.

McGuire, W.J., 1996. Volcano instability: a review of contemporary themes. Geol. Soc. (Lond.) Spec. Publ. 110 (1), 1–23. https://doi.org/10.1144/GSL.SP.1996.110.01.01.

McMurtry, G.M., Fryer, G.J., Tappin, D.R., Wilkinson, I.P., Williams, M., Fietzke, J., Garbe-Schoenberg, D., Watts, P., 2004. Megatsunami deposits on Kohala volcano, Hawaii, from flank collapse of Mauna Loa. Geology 32 (9), 741–744. https://doi.org/10.1130/G20642.1.

Melo, C.S., Ramalho, R.S., Quartau, R., Hipólito, A.R., Gill, A., Borges, P.A., Cardigos, F., Avila, S.P., Madeira, J., Gaspar, J.L., 2018. Genesis and morphological evolution of coastal talus-platforms (fajãs) with lagoon systems: the case study of the newly-formed Fajã dos Milagres (Corvo Island, Azores). Geomorphology 310, 138–152. https://doi.org/10.1016/j.geomorph.2018.03.006.

Mitchell, N.C., Beier, C., Rosin, P.L., Quartau, R., Tempera, F., 2008. Lava penetrating water: submarine lava flows around the coasts of Pico Island, Azores. Geochem. Geophys. Geosyst. 9 (3), Q03024. https://doi.org/10.1029/2007GC001725.

Moore, J.G., Normark, W.R., Holcomb, R.T., 1994. Giant Hawaiian underwater landslides. Science 264 (5155), 46–48. https://doi.org/10.1126/science.264.5155.46.

Moore, J.G., Bryan, W.B., Beeson, M.H., Normark, W.R., 1995. Giant blocks in the South Kona landslide, Hawaii. Geology 23, 125–128. https://doi.org/10.1130/0091-7613(1995)023<0125:GBITSK>2.3.CO;2.

Omira, R., Quartau, R., Ramalho, I., Baptista, M.A., Neil, M., 2016a. The tsunami effects of a collapse of a volcanic island on a semi-enclosed basin. In: Duarte, J., Schellart, W. (Eds.), The Pico-São Jorge Channel in the Azores Archipelago. In: Plate Boundaries and Natural Hazards. American Geophysical Union (AGU), John Wiley & Sons. ISBN 978-1-119-05397-2, pp. 271–283.

Omira, R., Baptista, M.A., Lisboa, F., 2016b. Tsunami characteristics along the Peru–Chile trench: analysis of the 2015 Mw 8. 3 Illapel, the 2014 Mw 8. 2 Iquique and

the 2010 Mw 8. 8 Maule tsunamis in the near-field. Pure Appl. Geophys. 173 (4), 1063–1077. https://doi.org/10.1007/s00024-016-1277-0.

Omira, R., Ramalho, I., 2020. Evidence-calibrated numerical model of December 22, 2018, Anak Krakatau flank collapse and tsunami. Pure Appl. Geophys. 177, 3059–3071. https://doi.org/10.1007/s00024-020-02532-x.

Paris, A., Heinrich, P., Paris, R., Abadie, S., 2020. The December 22, 2018 Anak Krakatau, Indonesia, landslide and tsunami: preliminary modeling results. Pure Appl. Geophys. 177, 571–590. https://doi.org/10.1007/s00024-019-02394-y.

Paris, R., Giachetti, T., Chevalier, J., Guillou, H., Frank, N., 2011. Tsunami deposits in Santiago Island (Cape Verde archipelago) as possible evidence of a massive flank failure of Fogos volcano. Sediment. Geol. 239 (3–4), 129–145. https://doi.org/10.1016/j.sedgeo.2011.06.006.

Paris, R., Bravo, J.J.C., González, M.E.M., Kelfoun, K., Nauret, F., 2017. Explosive eruption, flank collapse and megatsunami at Tenerife ca. 170 ka. Nat. Commun. 8, 15246. https://doi.org/10.1038/ncomms15246.

Paris, R., Ramalho, R.S., Madeira, J., Ávila, S., May, S.M., Rixhon, G., Engel, M., Brückner, H., Herzog, M., Schukraft, G., Perez-Torrado, F.J., 2018. Mega-tsunami conglomerates and flank collapses of ocean island volcanoes. Mar. Geol. 395, 168–187. https://doi.org/10.1016/j.margeo.2017.10.004.

Pérez-Torrado, F.J., Paris, R., Cabrera, M.C., Schneider, J.-L., Wassmer, P., Carracedo, J.-C., Rodríguez-Santana, Á., Santana, F., 2006. Tsunami deposits related to flank collapse in oceanic volcanoes: the Agaete Valley evidence, Gran Canaria, Canary Islands. Mar. Geol. 227, 135–149. https://doi.org/10.1016/j.margeo.2005.11.008.

Putra, P.S., Aswan, A., Maryunani, K.A., Yulianto, E., Nugroho, S.H., Setiawan, V., 2020. Post-event field survey of the 22 December 2018 Anak Krakatau tsunami. Pure Appl. Geophys. 177, 2477–2492. https://doi.org/10.1007/s00024-020-02446-8.

Quartau, R., Trenhaile, A.S., Mitchell, N.C., Tempera, F., 2010. Development of volcanic insular shelves: insights from observations and modelling of Faial Island in the Azores archipelago. Mar. Geol. 275, 66–83. https://doi.org/10.1016/j.margeo.2010.04.008.

Quartau, R., Madeira, J., Mitchell, N.C., Tempera, F., Silva, P.F., Brandão, F., 2015. The insular shelves of the Faial-Pico Ridge: a morphological record of its geologic evolution (Azores archipelago). Geochem. Geophys. Geosyst. 16, 1401–1420. https://doi.org/10.1002/2015GC005733.

Quartau, R., Ramalho, R.S., Madeira, J., Santos, R., Rodrigues, A., Roque, C., Carrara, G., da Silveira, A.B., 2018a. Gravitational, erosional and depositional processes on volcanic ocean islands: insights from the submarine morphology of Madeira archipelago. Earth Planet. Sci. Lett. 482, 288–299. https://doi.org/10.1016/j.epsl.2017.11.003.

Quartau, R., Trenhaile, A.S., Ramalho, R.S., Mitchell, N.C., 2018b. The role of subsidence in shelf widening around ocean island volcanoes: insights from observed morphology and modeling. Earth Planet. Sci. Lett. 498, 408–417. https://doi.org/10.1016/j.epsl.2018.07.007.

Ramalho, R.S., Winckler, G., Madeira, J., Helffrich, G.R., Hipólito, A., Quartau Adena, K., Schaefer, J.M., 2015a. Hazard potential of volcanic flank collapses raised by new megatsunami evidence. Sci. Adv. 1 (9), e1500456. https://doi.org/10.1126/sciadv.1500456.

Ramalho, R.S., Brum da Silveira, A., Fonseca, P., Madeira, J., Cosca, M., Cachão, M., Fonseca, M., Prada, S., 2015b. The emergence of volcanic oceanic islands on a slow-moving plate: the example of Madeira Island, NE Atlantic. Geochem. Geophys. Geosyst., 522–537. https://doi.org/10.1002/2014GC005657.

Ramalho, R.S., Quartau, R., Trenhaile, A.S., Mitchell, N.C., Woodroffe, C.D., Avila, S.P., 2013. Coastal evolution on volcanic oceanic islands: a complex interplay between volcanism, erosion, sedimentation, sea-level change and biogenic production. Earth-Sci. Rev. 127, 140–170. https://doi.org/10.1016/j.earscirev.2013.10.007.

Rodrigues, D.M.M., 2005. Análise de risco de movimentos de vertente e ordenamento do território na Madeira: aplicação ao caso de Machico. PhD thesis. Universidade da Madeira, Funchal. p. 382.

Rosser, N.J., Brain, M.J., Petley, D.N., Lim, M., Norman, E.C., 2013. Coastline retreat via progressive failure of rocky coastal cliffs. Geology 41 (8), 939–942.

Rusu, E., Onea, F., 2016. Estimation of the wave energy conversion efficiency in the Atlantic Ocean close to the European islands. Renew. Energy 85, 687–703.

Sansone, F.J., Smith, J.R., 2006. Rapid mass wasting following nearshore submarine volcanism on Kilauea volcano, Hawaii. J. Volcanol. Geotherm. Res. 151 (1–3), 133–139. https://doi.org/10.1016/j.jvolgeores.2005.07.026.

Siebert, L., 1992. Threats from debris avalanches. Nature 356 (6371), 658–659. https://doi.org/10.1038/356658a0.

Stephenson, W., 2014. Rock coasts. In: Masselink, D., Gehrels, R. (Eds.), Coastal Environments and Global Change, first edition. John Wiley & Sons, pp. 356–379.

Tinti, S., Pagnoni, G., Zaniboni, F., 2006. The landslides and tsunamis of the 30th of December 2002 in Stromboli analysed through numerical simulations. Bull. Volcanol. 68 (5), 462–479. https://doi.org/10.1007/s00445-005-0022-9.

Trenhaile, A.S., 2014. Climate change and its impact on rock coasts. Chapter 2 in Rock Coast Geomorphology: a Global Synthesis. In: Kennedy, D.M., Stephenson, W.J., Naylor, L.A. (Eds.), Geological Society. London, Memoirs, vol. 40, pp. 7–17.

Völker, D.J., 2010. A simple and efficient GIS tool for volume calculations of submarine landslides. Geo Mar. Lett. 30, 541–547. https://doi.org/10.1007/s00367-009-0176-0.

Ward, S.N., Day, S., 2001. Cumbre Vieja volcano—potential collapse and tsunami at La Palma, Canary Islands. Geophys. Res. Lett. 28, 3397–3400. https://doi.org/10.1029/2001GL013110.

Watt, S.F.L., Talling, P.J., Vardy, M.E., Heller, V., Hühnerbach, V., Urlaub, M., Sarkar, S., Masson, D.G., Henstock, T.J., Minshull, T.A., Paulatto, M., 2012. Combinations of volcanic-flank and seafloor-sediment failure offshore Montserrat, and their implications for tsunami generation. Earth Planet. Sci. Lett. 319, 228–240. https://doi.org/10.1016/j.epsl.2011.11.032.

Zengaffinen, T., Løvholt, F., Pedersen, G.K., Muhari, A., 2020. Modelling 2018 Anak Krakatoa flank collapse and tsunami: effect of landslide failure mechanism and dynamics on tsunami generation. Pure Appl. Geophys. 177 (6), 2493–2516. https://doi.org/10.1007/s00024-020-02489-x.